Progress In Electromagnetics Research, Vol. 128, 479–502, 2012

BISTATIC FMCW SAR RAW SIGNAL SIMULATOR FOR EXTENDED SCENES

Y. Liu*, Y. Deng, R. Wang, and X. Jia

Spaceborne Microwave Remote Sensing System Department, Institute of Electronics, Chinese Academy of Sciences (IECAS), Beijing, China

Abstract—By mounting the transmitter and receiver of Frequency Modulated Continuous Wave (FMCW) Synthetic Aperture Radar (SAR) system on separate platforms, bistatic FMCW SAR offers more considerable capabilities, reliability and flexibility while maintaining the small size, low cost and agile reaction. The bistatic FMCW SAR raw signal simulator is highly required to quantitatively support the design of bistatic FMCW SAR, to help mission planning, test processing algorithms, and analyze jamming and noises. Bistatic FMCW SAR raw signal can be exactly simulated target-by-target in time domain but with extremely time and memory consuming, especially when extended scenes are considered. In this paper, bistatic FMCW SAR signal model and Bistatic Point Target Reference Spectrum (BPTRS) is proposed, based on which a raw signal simulator is developed in the 2-D frequency domain for the first time, where Chirp-Z Transform (CZT) is used to formulate the range migration terms. By taking advantage of Fast Fourier Transform (FFT), the proposed raw signal simulator highly reduces the computational load with respect to the time domain approach. The simulated raw data is verified by analyzing the corresponding images focused by Range Doppler Algorithm (RDA).

1. INTRODUCTION

By transmitting Frequency-Modulated Continuous-Wave (FMCW), FMCW Synthetic Aperture Radar (SAR) makes a lightweight and cost-effective remote sensing instrument of high resolution which can work all weather, day and night [1–11]. FMCW SAR system simplifies the transmitter design, increases both performance and reliability as well

Received 16 April 2012, Accepted 29 May 2012, Scheduled 6 June 2012

* Corresponding author: Yue Liu (liuyuehappy@gmail.com).

as reduces the risk of breakdown or arcing in the high power cables, by extending the pulse duration to reduce the transmitter peak power requirements, without degrading either the resolution or SNR [12]. With the smaller-size, lower-cost and more agile reaction, FMCW SAR is of great interest to the civil market and military applications [1–11]. In the recent ten years, there are already several successful FMCW SAR systems that have made great contributions to the remote sensing fields [8–11].

FMCW SAR is based on continuously transmitting and receiving the modulated signal (i.e., 100% duty cycle) — which usually demand separate dedicated transmitter and receiver [11]. But it causes great trouble to achieve the antenna isolation if two separate antennas are used on one platform [11]. By allocating the radar transmitter and receiver on separate platforms, bistatic FMCW SAR can overcome the antenna isolation problem. Moreover, it is an extension of the traditional monostatic FMCW SAR with increased capabilities, reliability and flexibility [13–24], while keeping the advantages of small size, low cost and agile reaction. Bistatic FMCW SAR have a great potential for remote sensing applications in airborne and spaceborne remote sensing fields, such as frequent monitoring, high resolution imaging, wide-swath detecting, scene classification, and single pass cross-track interferometry, especially where frequent revisits at low cost are needed or where small size is required [13–24]. Thus the subject of design, processing, and data interpretation for the bistatic FMCW SAR mode is gaining an increasingly wide interest in the remote sensing scientific community.

Therefore, to quantitatively support the design of bistatic FMCW SAR, to help mission planning, to test processing algorithms, and to analyze jamming and noises, a bistatic FMCW SAR raw signal simulator is required [25–33], especially when the real system is not ready yet. Time-domain SAR raw signal simulator can be easily developed by a twofold integral of reflectivity and impulse response function, which is able to deal with point targets or small scenes, because it will be enormously time and memory consuming when extended scenes are considered. Conversely, to the best of our knowledge, no frequency-domain simulators are currently available for the bistatic FMCW SAR mode. However, simulation of bistatic FMCW SAR raw signals from extended scenes is highly desirable with system design and mission planning, because it is capable of analyzing the effects of different design and mission parameter choices for different kinds of imaged scenes [25–33].

In this paper, a bistatic FMCW SAR raw signal simulation approach is developed in the 2-D frequency domain for the first

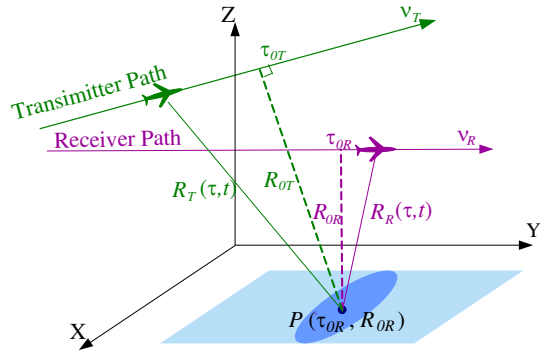

Figure 1. Bistatic FMCW SAR geometry.

time. The approach is based on the proposed accurate bistatic FMCW SAR signal model and Bistatic Point Target Reference Spectrum (BPTRS). Chirp-Z Transform (CZT) is used to accurately formulate the range-variant Range Cell Migration (RCM) without any interpolation operations [34, 35]. Taking advantage of Fast Fourier Transform (FFT), the proposed simulation approach highly reduces the computational load with respect to a time domain raw signal simulator. The raw signal of point targets and an actual scene (Niederweidbach, Germany) is simulated and well focused by Range Doppler Algorithm (RDA). The computational complexity of the proposed approach is calculated and shows remarkable reduction compared with that of the time-domain method.

This paper is organized as follows. The bistatic FMCW SAR signal model is developed in both time domain and frequency domain in Section 2. Section 3 proposes the theory of the raw signal simulation approach in bistatic FMCW SAR configuration based on the signal models. Section 4 shows the processing result of simulated raw signal. The computational complexity is analyzed and compared in Section 5. Conclusions are reported in Section 6.

2. BISTATIC FMCW SAR SIGNAL MODEL AND BPTRS

In this section, the bistatic FMCW SAR echoed signal of a point target is formulated in both time domain and frequency domain, in order to derive an efficient frequency domain approach for bistatic FMCW SAR raw signal simulation. The bistatic FMCW SAR geometry is shown as Fig. 1. The mathematical symbols and their definitions used in this paper are given as follows.

t, τ	Range and Azimuth time variables
$f,\ f_\tau$	Range and Azimuth frequency variables
f_0	Carrier frequency
K_r	Chirp rate
T_r	Pulse duration
B_r	Range bandwidth
$\tau_{0T},\ \tau_{0R}$	zero Doppler times of the receiver and transmitter
$R_{0T},\ R_{0R}$	closest slant ranges from transmitter and receiver to the point target $P(\tau_{0R}, R_{0R})$
$\tau_{0R},\ R_{0R}$	receiver-referenced coordinates, defined as the coordinates of image space
$\sigma(\tau_{0R}, R_{0R})$	Backscattering coefficient of the target $P(\tau_{R0}, R_{R0})$
c	Signal transfer velocity
$v_T,\ v_R$	Platform velocities of the receiver and transmitter
r_c	Reference range for dechirp operation
$W_a,\ W_r$	Antenna beam pattern in the azimuth and range directions
$N_a,\ N_r$	Sampling number in azimuth and range directions

Here we assume the transmitted signal is a chirp modulation in the following formulation [36],

$$s(\tau, t) = \exp\left(j\pi K_r t^2\right) \tag{1}$$

In the case of the Continuous-Wave (CW) SAR, however, the commonly used stop-and-go approximation no longer holds due to the continuous move during the long pulse time [1], thus the instantaneous slant ranges are determined by both the range and azimuth variables. The round-trip delay time τ_d of the target $P(\tau_{R0}, R_{R0})$ is express as,

$$\tau_d = \frac{R_T(\tau, t) + R_R(\tau, t)}{c} \tag{2}$$

where

$$R_T(\tau, t) = \sqrt{R_{0T}^2 + (\tau + t - \tau_{0T})^2 v_T^2} \tag{3}$$

$$R_R(\tau, t) = \sqrt{R_{0R}^2 + (\tau + t - \tau_{0R})^2 v_R^2} \tag{4}$$

Neglecting the time scaling influence on the pulse envelope, the echoed signal from $P(\tau_{R0}, R_{R0})$ is expressed as [36],

$$g_0(\tau, t) = \sigma(\tau_{0R}, R_{0R}) s(t - \tau_d) \exp\left[-j2\pi f_0 (t - \tau_d)\right] \tag{5}$$

The signal is transmitted at the time $\tau = nT_r$, where n denotes the period number [1]. The transmitted signal is synchronized by the repetition period.

The pulse duration of FMCW SAR is thousands of times as that of pulsed SAR, so dechirp-on-receive technology is generally used in the FMCW SAR system to reduce the sampling requirements and data rate [8–10]. The reference signal for dechirp processing is formulated as

$$g_{ref}(\tau, t, \tau_c) = s^*(t - \tau_c) \exp[j2\pi f_0 (t - \tau_c)] \tag{6}$$

where $s^*(t)$ denotes the conjugate of the transmitted signal. The reference time delay is defined as $\tau_c = 2r_c/c$. After dechirp operation, the echoed signal from $P(\tau_{R0}, R_{R0})$ is expressed as $g(\tau, t)$, i.e.,

$$\begin{aligned} g(\tau, t) = {} & \sigma(\tau_{0R}, R_{0R}) \exp[-j2\pi f_0 (\tau_d - \tau_c)] \\ & \exp[-j2\pi K_r (t - \tau_c)(\tau_d - \tau_c)] \exp\left[-j2\pi K_r (\tau_d - \tau_c)^2\right] \end{aligned} \tag{7}$$

In order to derive an efficient frequency domain approach to simulate the bistatic FMCW SAR raw signal, the BPTRS for FMCW configuration is highly desirable. The basis of developing the BPTRS is the point target signal model $g(\tau, t)$, as shown in (7). The first step is to remove the last exponential term of (7), which is well known as the Residual Video Phase (RVP). This takes three steps, range Fourier Transformation (FT), phase multiplication, and range Inverse FT (IFT) [12]. After RVP is removed, the echoed signal from $P(\tau_{R0}, R_{R0})$ is expressed as,

$$\begin{aligned} g_1(\tau, t) = {} & \sigma(\tau_{0R}, R_{0R}) \exp[-j2\pi f_0 (\tau_d - \tau_c)] \\ & \exp[-j2\pi K_r (t - \tau_c)(\tau_d - \tau_c)] \end{aligned} \tag{8}$$

Then we perform the time–frequency substitution of $f = K_r (t - \tau_c)$ to segment $g_1(\tau, t)$ into the azimuth-time and range-frequency domain, which is formulated as,

$$g_1(\tau, f) = \sigma(\tau_{0R}, R_{0R}) \exp\{-j2\pi (f + f_0)(\tau_d - \tau_c)\} \tag{9}$$

To obtain the desired BPTRS, we apply FT to $g_1(\tau, f)$ with respect to the azimuth time variable τ, i.e.,

$$\begin{aligned} G(f_\tau, f) = {} & \int_{-\infty}^{\infty} g_1(\tau, f) \exp(-j2\pi f_\tau \tau)\, d\tau \\ = {} & \sigma(\tau_{0R}, R_{0R}) \int_{-\infty}^{\infty} \exp\{-j\Phi(\tau, t, f, f_\tau)\}\, d\tau \end{aligned} \tag{10}$$

where

$$\Phi(\tau, t, f, f_\tau) = 2\pi (f + f_0) \left[\frac{R_T(\tau, t)}{c} + \frac{R_R(\tau, t)}{c} - \frac{2r_c}{c}\right] + 2\pi f_\tau \tau \tag{11}$$

Consequently, the principle of stationary phase can be readily applied to obtain the solution of the integral in (10) to derive the

desired BPTRS. At the point of stationary phase τ_s, the first derivative of the phase $\Phi(\tau, t, f, f_\tau)$ is zero [23, 36], i.e.,

$$\left.\frac{d\Phi(\tau, t, f, f_\tau)}{d\tau}\right|_{\tau = \tau_s} = 0 \tag{12}$$

Thus the Doppler frequency f_τ and the point of stationary phase τ_s can be related as,

$$f_\tau = -\frac{(f + f_0)}{c}\left[\frac{v_T^2(\tau_s + t - \tau_{0T})}{R_T(\tau_s, t)} + \frac{v_R^2(\tau_s + t - \tau_{0R})}{R_R(\tau_s, t)}\right] \tag{13}$$

Equation (13) contains Double Square Roots (DSR) so it is difficult to directly achieve the analytical relation between the Doppler frequency and the point of stationary phase [14–23]. To circumvent this limitation, we decompose f_τ into two parts where each of them is related to τ_s by a single square root. For notational convenience, we express the Doppler frequency as a receiver and transmitter contribution, writing

$$f_\tau = f_{\tau T} + f_{\tau R} \tag{14}$$

where

$$f_{\tau T} = -\frac{(f_0 + f)}{c}\left[\frac{v_T^2(\tau_s + t - \tau_{0T})}{R_T(\tau_s, t)}\right] \tag{15}$$

$$f_{\tau R} = -\frac{(f_0 + f)}{c}\left[\frac{v_R^2(\tau_s + t - \tau_{0R})}{R_R(\tau_s, t)}\right] \tag{16}$$

Solving (15) and (16), we can formulate the slant trajectories of the transmitter and receiver in the two-dimensional frequency domain, respectively,

$$R_T(f_{\tau T}, f) = \frac{R_{0T}}{\sqrt{1 - \frac{c^2 f_{\tau T}^2}{v_T^2 (f_0 + f)^2}}} \tag{17}$$

$$R_R(f_{\tau R}, f) = \frac{R_{0R}}{\sqrt{1 - \frac{c^2 f_{\tau R}^2}{v_R^2 (f_0 + f)^2}}} \tag{18}$$

Substituting (17) and (18) into (13) yields,

$$f_\tau = \frac{(f + f_0)}{c}\left[\frac{v_T^2(\tau_s + t - \tau_{0T})}{R_T(f_{\tau T}, f)} + \frac{v_R^2(\tau_s + t - \tau_{0R})}{R_R(f_{\tau R}, f)}\right] \tag{19}$$

Consequently, the analytical expression of the point of stationary phase can be developed by solving (19) for τ_s, i.e.,

$$\tau_s = \frac{\begin{array}{l}\frac{cf_\tau}{(f_0+f)} R_R(f_{\tau R}, f) R_T(f_{\tau T}, f) \\ + R_R(f_{\tau R}, f) v_T^2 \tau_{0T} + R_T(f_{\tau T}, f) v_R^2 \tau_{0R}\end{array}}{R_R(f_{\tau R}, f) v_T^2 + R_T(f_{\tau T}, f) v_R^2} - \frac{f}{K_r} - \tau_c \tag{20}$$

Substituting (20) into the right side of (15) and (16) for τ_s, respectively, we achieve,

$$f_{\tau T} = \frac{R_{0R}v_T^2}{R_{0T}v_R^2 + R_{0R}v_T^2} f_\tau + \frac{(f_0+f)}{c} \frac{v_T^2 v_R^2 (\tau_{0R} - \tau_{0T})}{R_{0T}v_R^2 + R_{0R}v_T^2} \tag{21}$$

$$f_{\tau R} = \frac{R_{0T}v_R^2}{R_{0T}v_R^2 + R_{0R}v_T^2} f_\tau + \frac{(f_0+f)}{c} \frac{v_T^2 v_R^2 (\tau_{0T} - \tau_{0R})}{R_{0T}v_R^2 + R_{0R}v_T^2} \tag{22}$$

Note that the Doppler modulation rates introduced by the motion of transmitter and receiver are different. According to the principle of stationary phase [22, 23, 36], substituting τ_s in (20) on the right side of (11) for τ gives the desired bistatic FMCW SAR BPTRS, which is expressed as,

$$G(f_\tau, f) = \sigma(\tau_{0R}, R_{0R}) \exp[-j\Phi(f_\tau, f)] \tag{23}$$

where

$$\begin{aligned}
&\Phi(f_\tau, f) \\
&= \frac{2\pi R_{0T}}{c} \sqrt{(f_0+f)^2 - \left(\frac{cf_{\tau T}}{v_T}\right)^2} + \frac{2\pi R_{0R}}{c} \sqrt{(f_0+f)^2 - \left(\frac{cf_{\tau R}}{v_R}\right)^2} \\
&\quad - 2\pi f_\tau \frac{f}{K_r} + 2\pi f_\tau \frac{R_{0R}v_T^2\tau_{0T} + R_{0T}v_R^2\tau_{0R}}{R_{0R}v_T^2 + R_{0T}v_R^2} - 4\pi(f_0+f)\frac{r_c}{c} - 4\pi f_\tau \frac{r_c}{c}
\end{aligned} \tag{24}$$

Before developing an approach to simulate the raw data, we should understand the characteristics of this bistatic FMCW SAR spectrum, i.e.,

1) Equation (24) contains an additional term $-2\pi f_\tau f/K_r$, which does not present in the pulsed SAR BPTRS. This term is introduced by the variation of the slant range during the long pulse duration. The coupling term is the essential difference between this proposed spectrum and the one for pulsed SAR. Since this term is range-invariant, it can be simulated via a Reference Function Multiplication (RFM).
2) The proposed bistatic FMCW SAR spectrum contains another two range-invariant terms, i.e., $(-4\pi(f_0+f)r_c/c$ and $-4\pi f_\tau r_c/c)$, which are introduced by the dechirp-on-receive operation, and refer to the constant range and azimuth shifts, respectively, thus they can also be simulated by RFM operation.
3) The fourth term (i.e., $2\pi f_\tau \frac{R_{0R}v_T^2\tau_{0T} + R_{0T}v_R^2\tau_{0R}}{R_{0R}v_T^2 + R_{0T}v_R^2}$) is dependent on the zero-Doppler time of the transmitter and receiver, which determines by the azimuth registration position of the target.

4) If we set $R_{0T} = R_{0R}$, $v_T = v_R$, $\tau_{0T} = \tau_{0R}$ where the bistatic FMCW SAR configuration reduces to a monostatic case, the FMCW BPTRS (24) will be the same as the monostatic FMCW SAR spectrum [1].

However, for the bistatic configuration, because of the double square roots variant with the slant range from the target to the transmitter and receiver, the bistatic range history is in the form of a Flat Top Hyperbola (FTH). To propose the raw signal simulation approach, the bistatic FMCW SAR spectrum model is reformulated by a geometric transformation method [24], in order to be prepared for proposing a high efficient raw signal simulation approach. Note that R_{0R} can be expressed as the sum of a linearly variant term r and invariant term

$$R_{0R} = R_{mR} + r \tag{25}$$

where R_{mR} denotes the closest range from the scene center to the receiver path, r denotes the zero-offset receiver-to-target range variable [24].

The geometric image transformation is used to map R_{0T} onto R_{0R} and further express R_{0T} as a function of R_{0R} and r. According to Fig. 2, the one-to-one relationship between R_{0T} and R_{0R} can be formulated as [24]

$$R_{0T} = \sqrt{\left[\sqrt{(R_{mR} + r)^2 - H_{0R}^2} + d\right]^2 + H_{0T}^2} \tag{26}$$

where d is the projection of constant offsets between the transmitter and receiver in the range direction.

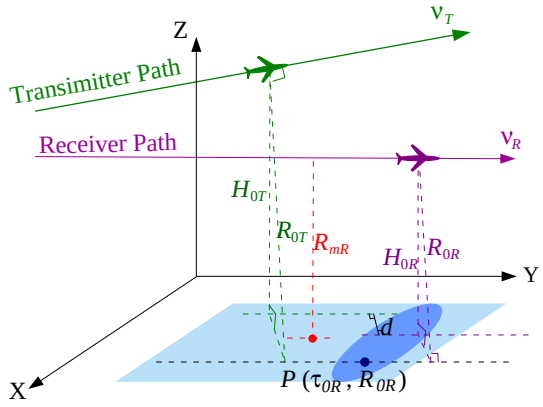

Figure 2. Geometric image transformation map.

Expanding (26) as the first-order Taylor series in terms of r/R_{mR} yields

$$R_{0T} = \alpha R_{mR} + \beta r \tag{27}$$

where

$$\begin{cases} \alpha = \sqrt{\left[\sqrt{1-\left(\frac{H_{0R}}{R_{mR}}\right)^2}+\frac{d}{R_{mR}}\right]^2+\left(\frac{H_{0T}}{R_{mR}}\right)^2} \\ \beta = \frac{R_{mR}+\frac{R_{mR}}{\sqrt{R_{mR}^2-H_{0R}^2}}}{\sqrt{\left(\sqrt{R_{mR}^2-H_{0R}^2}+d\right)^2+H_{0T}^2}} \end{cases} \tag{28}$$

Thus the phase of the proposed signal spectrum $G(f_\tau, f)$ can be reformulated as,

$$\begin{aligned} &\Phi(f, f_\tau) \\ &= \frac{2\pi(R_{0R}-R_{mR})}{c}\left\{\beta\sqrt{(f_0+f)^2-\left(\frac{cf_{\tau T}}{v_T}\right)^2}+\sqrt{(f_0+f)^2-\left(\frac{cf_{\tau R}}{v_R}\right)^2}\right\} \\ &\quad+\frac{2\pi R_{mR}}{c}\left\{\alpha\sqrt{(f_0+f)^2-\left(\frac{cf_{\tau T}}{v_T}\right)^2}+\sqrt{(f_0+f)^2-\left(\frac{cf_{\tau R}}{v_R}\right)^2}\right\} \\ &\quad-2\pi f_\tau\frac{f}{K_r}+2\pi f_\tau\tau_0-4\pi(f_0+f)\frac{r_c}{c}-4\pi f_\tau\frac{r_c}{c} \end{aligned} \tag{29}$$

where

$$\tau_0 = \frac{R_{0R}v_T^2\tau_{0T}+R_{0T}v_R^2\tau_{0R}}{R_{0R}v_T^2+R_{0T}v_R^2} \tag{30}$$

From (29), we can see that the square root terms are divided into two parts, one is variant with the shortest slant range from the target to the receiver, and the other one refers to the constant range and azimuth coupling components, which can also be simulated by RFM operation.

For the range-variant term, the involved azimuth modulation components can be better understood by expanding the square roots using a Taylor series. Keeping the phase terms up to the first-order, i.e.,

$$\begin{aligned} \Phi(f, f_\tau) \approx{}& \frac{2\pi(R_{0R}-R_{mR})}{c}\{\Phi_0(f_{\tau T}, f_{\tau R})+\Phi_1(f_{\tau T}, f_{\tau R})f\} \\ &+\frac{2\pi R_{mR}}{c}\left\{\alpha\sqrt{(f_0+f)^2-\left(\frac{cf_{\tau T}}{v_T}\right)^2}+\sqrt{(f_0+f)^2-\left(\frac{cf_{\tau R}}{v_R}\right)^2}\right\} \end{aligned}$$

$$-2\pi f_\tau \frac{f}{K_r} + 2\pi f_\tau \tau_0 - 4\pi \left(f_0 + f\right) \frac{r_c}{c} - 4\pi f_\tau \frac{r_c}{c} \tag{31}$$

where

$$\begin{cases} \mu_T = \left(\frac{cf_{\tau T}}{v_T f_0}\right), \ D_T = \sqrt{1-\mu_T^2} \\ \mu_R = \left(\frac{cf_{\tau R}}{v_R f_0}\right), \ D_R = \sqrt{1-\mu_R^2} \end{cases} \tag{32}$$

$$\Phi_0\left(f_{\tau T}, f_{\tau R}\right) = \left(\beta D_T + D_R\right) f_0, \ \Phi_1\left(f_{\tau T}, f_{\tau R}\right) = \frac{\beta}{D_T} + \frac{1}{D_R} \tag{33}$$

The accuracy of this approximate formulation will be verified in Appendix A.

3. BISTATIC FMCW SAR RAW SIGNALS SIMULATION THEORY

In the case of extended scene, the bistatic FMCW SAR raw signal can be formulated as $g_{scene}\left(\tau, t\right)$ in time domain via integrating the echoed signal of the whole illuminated scene target-by-target, i.e.,

$$\begin{aligned} g_{scene}\left(\tau, t\right) \ = \ & \int_{R_{0R\text{near}}}^{R_{0R\text{far}}} \int_{\tau_{0R\,\min}}^{\tau_{0R\,\max}} W_a\left(\tau\right) W_r\left(t\right) rect\left[\frac{t-\tau_d}{T_r}\right] \\ & g\left(\tau, t\right) d\tau_{0R} dR_{0R} \end{aligned} \tag{34}$$

where $\tau_{oR\,\min}$ and $\tau_{oR\,\max}$ represent the minimal and the maximal zero-Doppler time in the illuminated scene, and $R_{oR\text{near}}$ and $R_{oR\text{far}}$ represent the nearest and farthest slant range, respectively.

The simulated bistatic FMCW SAR raw signal for extended scene can be obtained following (34) in time domain, which demands twofold integral of the reflectivity and impulse response functions. The consumption of time and memory is only acceptable for simulations of point targets or small scenes, but not when extended scenes are considered [25–33]. To help with bistatic FMCW SAR system design, mission planning and parameter choices, an efficient bistatic FMCW SAR raw signal simulator for extended scenes is needed, which has to be developed in the frequency domain.

The idea of developing a high efficient bistatic FMCW SAR raw signal simulator for an extended scene is by formulating the corresponding spectrum first, and then the desired signal can be simulated through inverse FFT. The basis of simulating the spectrum is the FMCW SAR BPTRS. Based on the aforementioned reformulation of BPTRS, as shown in (31), a high efficient raw signal simulation approach for bistatic FMCW SAR is ready to be proposed in the two-dimensional frequency domain. The signal simulation procedure is

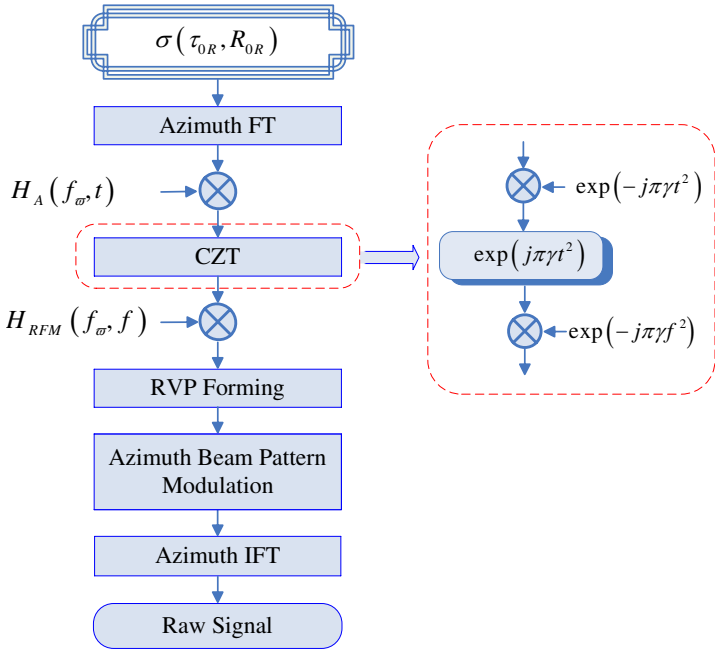

Figure 3. Bistatic FMCW SAR raw signal simulation procedure.

shown in the block diagram in Fig. 3, and its basic operations are illustrated as follows.

3.1. Reflectivity Mapping

To achieve the reflectivity map, the reflectivity has to be located at the right position of the image plane. It needs to be multiplied by a phase term caused by the propagation time delay. Instead of the entire propagation time, the multiplied phase here represents the delay time from the receiver to the target corresponding to the scene center as shown in (12), which is expressed:

$$t_0 = \frac{2\left(R_{0T} - R_{mT} + R_{0R} - R_{mR}\right)}{c} \tag{35}$$

After reflectivity mapping, the data can be expressed as

$$g_F(\tau, t) = \int_{R_{0R\text{near}}}^{R_{0R\text{far}}} \int_{\tau_{0R\,\min}}^{\tau_{0R\,\max}} G_r(t)\,\sigma(\tau_{0R}, R_{0R}) p_a(\tau - \tau_0)\, p_r(t - t_0)\, d\tau_{0R} dR_{0R} \tag{36}$$

where $p_a(\tau)$ and $p_r(t)$ represent the sinc-like pulse envelope in the azimuth and range directions, respectively.

3.2. Azimuth FFT

Apply Azimuth FFT operation to the simulated scenario to transform the signal into the Range-Doppler (RD) domain, thus the signal becomes

$$G_F(f_\tau, t) = \int_{R_{0R\text{near}}}^{R_{0R\text{far}}} \int_{\tau_{0R\,\min}}^{\tau_{0R\,\max}} G_r(f)\,\sigma(\tau_{0R}, R_{0R})\,p_r(t-t_0) \exp(-j2\pi f_\tau \tau_0)\,d\tau_{0R} dR_{0R} \tag{37}$$

The azimuth frequency axes should be set for the simulated signal. To accomplish this, the Doppler centroid has to be calculated first. In the broadside configuration, the azimuth Doppler centroid is zero. Nevertheless, in the squint configuration, the Doppler centroid is shifted by $v_T f_0 \sin\theta_T/c + v_R f_0 \sin\theta_R/c$. Generally the azimuth frequency can be set in the center $v_T f_0 \sin\theta_T/c + v_R f_0 \sin\theta_R/c$, where θ_T and θ_R denotes the squint angle of the transmitter and receiver, respectively.

3.3. Azimuth Residual Phase Simulation

The azimuth residual phase can be simulated in the RD domain by multiplying a function which is expressed as

$$H_A(f_{\tau T}, f_{\tau R}, t) = \exp\left(-j\frac{2\pi r}{c}(\beta D_T + D_R) f_0\right) \tag{38}$$

The signal after this operation is expressed as

$$\begin{aligned} G_A(f_\tau, t) &= \int_{R_{0R\text{near}}}^{R_{0R\text{far}}} \int_{\tau_{0R\,\min}}^{\tau_{0R\,\max}} G_r(f)\,\sigma(\tau_{0R}, R_{0R})\,p_r(t-t_0) \\ &\quad \exp\left(-j\frac{2\pi(R_{0R}-R_{ref})}{c}(\beta D_T + D_R) f_0 - j2\pi f_\tau \tau_0\right) d\tau_{0R} dR_{0R} \\ &= \int_{R_{0R\text{near}}}^{R_{0R\text{far}}} \int_{\tau_{0R\,\min}}^{\tau_{0R\,\max}} G_r(f)\,\sigma(\tau_{0R}, R_{0R})\,p_r(t-t_0) \\ &\quad \exp\left(-j\frac{2\pi(R_{0R}-R_{ref})}{c}\Phi_0 - j2\pi f_\tau \tau_0\right) d\tau_{0R} dR_{0R} \end{aligned} \tag{39}$$

where the reference range R_{ref} is generally chosen as the shortest slant range from the target to the receiver, i.e., R_{mR}.

3.4. Range-variant Range Cell Migration Simulation Based on CZT

CZT operation is ready to be carried out to simulate the range-variant range cell migration phase with respect to the distance from the target to receiver by forming the scaling factor in range,

$$G_{CZT}(f_\tau, f) = \int G_A(f_\tau, t) H(f_\tau, f, t)\, dt \tag{40}$$

The kernel is expressed as

$$H(f_\tau, f, t) = \exp(-j2\pi\gamma f t) \tag{41}$$

where the scaling factor γ is defined as

$$\gamma = \frac{\frac{\beta}{D_T} + \frac{1}{D_R}}{1+\beta} \tag{42}$$

This operation can be evaluated by CZT algorithm efficiently [34, 35]. Note that the transform kernel (41) can be reformulated as

$$H(f_\tau, f, t) = \exp\left\{j\pi\gamma\left[(f-t)^2 - f^2 - t^2\right]\right\} \tag{43}$$

Then, (40) can be redefined as

$$\begin{aligned} & G_{CZT}(f_\tau, f) \\ = \; & \exp\left(-j\pi\gamma f^2\right) \int G_A(f_\tau, t) \exp\left(-j\pi\gamma t^2\right) \exp\left[-j\pi\gamma (t-f)^2\right] dt \end{aligned} \tag{44}$$

Thus the CZT operation can be carried out through one convolution and two multiplications as shown in Fig. 3, which saves a lot of time and memory. The signal after CZT is in the 2D frequency domain which is expressed as,

$$\begin{aligned} G_{CZT}(f_\tau, f) = & \int_{R_{0R\text{near}}}^{R_{0R\text{far}}} \int_{\tau_{0R\min}}^{\tau_{0R\max}} G_r(f)\, \sigma(\tau_{0R}, R_{0R}) \\ & \exp\left\{-j\frac{2\pi(R_{0R}-R_{ref})}{c}\left[\Phi_0 + \gamma f\right] - j2\pi f_\tau \tau_0\right\} dR_{0R} d\tau_0 \end{aligned} \tag{45}$$

3.5. Reference Function Multiplication

Now that the range-variant range term is formulated, RFM is carried out to simulate all the range-invariant terms, including range walk, bulk RCM, bulk range azimuth coupling and higher-order

range compression, and the terms introduced by dechirp-on-receive operation. Thus, the reference function is expressed as

$$H_{RFM}(f_\tau, f) = \exp\left\{-j\left[\frac{2\pi R_{mR}}{c}\left\{\alpha\sqrt{(f_0+f)^2-\left(\frac{cf_{\tau T}}{v_T}\right)^2}+\sqrt{(f_0+f)^2-\left(\frac{cf_{\tau R}}{v_R}\right)^2}\right\}\right.\right.$$
$$\left.\left.-2\pi f_\tau\frac{f}{K_r}-4\pi(f_0+f)\frac{r_c}{c}-4\pi f_\tau\frac{r_c}{c}\right]\right\} \quad (46)$$

After the aforementioned operations, the 2D spectrum of FMCW SAR raw signal is conceived, which is expressed as

$$G(f_\tau, f) = \int_{R_{0R\text{near}}}^{R_{0R\text{far}}}\int_{\tau_{0R\min}}^{\tau_{0R\max}}\sigma(\tau_{0R}, R_{0R})\,G_r(f)\,rect\left[\frac{f}{B_r}\right] \exp\left[-j\Phi(f_\tau, f)\right]dR_{0R}d\tau_0 \quad (47)$$

where

$$\Phi(f, f_\tau) = \frac{2\pi R_{0T}}{c}\sqrt{(f_0+f)^2-\left(\frac{cf_{\tau T}}{v_T}\right)^2}+\frac{2\pi R_{0R}}{c}\sqrt{(f_0+f)^2-\left(\frac{cf_{\tau R}}{v_R}\right)^2}$$
$$-2\pi f_\tau\frac{f}{K_r}+2\pi f_\tau\tau_0-4\pi(f_0+f)\frac{r_c}{c}-4\pi f_\tau\frac{r_c}{c} \quad (48)$$

Hereto, the spectrum of FMCW SAR raw signal is simulated. Note that the proposed BPTRS is achieved after RVP removal, so RVP needs to be formed before achieving the accurate raw signal.

3.6. RVP Forming

Opposite to RVP correction which was described in the last section, besides the signal is in frequency domain, RVP forming needs two steps, phase multiplication, and Inverse FT (IFT) [36].

3.7. Azimuth Beam Pattern Modulation

To simulate the skewness of the spectrum in the frequency domain, the variance of the azimuth beam pattern $G_a(f_\tau)$ with the range frequency f should be taken into account. Otherwise, ignoring the variation will lead to the deviation of the supporting area of the raw signal from the ideal area in the time domain.

3.8. Azimuth IFFT

After all of the aforementioned operations, the bistatic FMCW SAR raw signal can be conceived by an azimuth Inverse Fourier Transform (IFT). Performing Azimuth IFT to (19), using stationary phase principle, the signal is expressed as

$$\begin{aligned} s(\tau,t) \;=\; & \int_{R_{0R\text{near}}}^{R_{0R\text{far}}} \int_{\tau_{0R\,\min}}^{\tau_{0R\,\max}} \sigma(\tau_0,R_0) G_a(\tau)\, G_r(t)\, rect\left[\frac{t-\tau_d}{T_r}\right] \\ & \exp\left[-j2\pi f_0(\tau_d-\tau_c)\right] \times \exp\left[-j2\pi K_r(\tau_d-\tau_c)(t-\tau_c)\right] \\ & \times \exp\left[-j2\pi K_r(\tau_d-\tau_c)^2\right] d\tau_0 dR_0 \end{aligned} \tag{49}$$

Comparing (49) with (34), we can see that the proposed frequency domain simulation approach achieves the bistatic FMCW SAR signal of extended scene with the same formulation of the target by target method in time domain. Note that this conclusion is based on the accuracy of the reformulation of the proposed BPTRS, i.e., Eq. (31), which is proved in Appendix A. Hereby the proposed bistatic FMCW SAR raw signal simulation is completed.

By taking advantage of fast Fourier transform (FFT), the proposed approach greatly reduces the computational load with respect to the target by target time domain raw signal simulation. Numerical analysis will be outlined in Section 5.

4. SIMULATION EXPERIMENTS

The best way to validate the accuracy of the proposed raw signal simulation approach is by evaluating the corresponding images. Firstly a simulation of point targets is carried out. The designed scene contains nine point targets, as shown in Fig. 4. PT5 is located in the scene center, PT4 and PT6 have the relative slant ranges: -150 and 150 m, and PT2 and PT8 have the relative zero-Doppler time: -0.2 s and 0.2 s, respectively, with respect to PT5 The backscattering coefficients of the targets are defined as "$1+j$", where j equals $\sqrt{-1}$. The simulation system parameters are shown in Table 1. To quantify the precision of processing, the impulse response width (IRW), peak sidelobe ratio (PSLR), and integrated sidelobe ratio (ISLR) are used as criteria. For the ongoing simulation, we assume the window functions of rectangular shape in both directions.

The bistatic FMCW SAR raw signal of the targets are simulated following the proposed frequency domain approach, and focused by RDA, as shown in Fig. 5 and the contour response of PT9 is shown in Fig. 5(b) for details. Figs. 5(c) and (d) compare the impulse

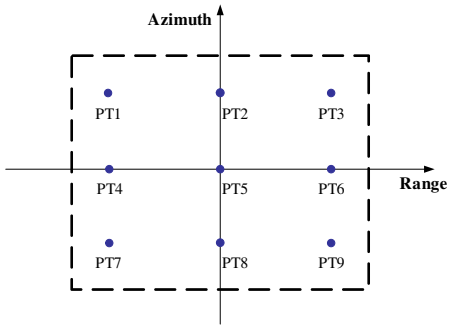

Figure 4. Scene geometry with nine point targets.

Table 1. System parameters.

	Transmitter	Receiver
Platform velocity	30 m/s	55 m/s
Platform altitude	1000 m	800 m
Mid-Swath slant range	1500 m	1120 m
Depression angle	48.19°	44.42°
Carrier frequency	10 GHz	
PRF	600 Hz	
Azimuth beamwidth	2.86°	
Swath Width	500 m	
Range bandwidth	500 MHz	

response of PT9 with that of the time domain method in azimuth and range, respectively. The measurements of target parameters are listed in Table 2, which agree well with the theoretical values. The measured IRWs in azimuth and range have a maximal broadening by a factor of 0.7%, which agree well with the theoretical values of 0.3 m in azimuth and 0.3 m in range. The two-dimensional ISLRs deviate from the theoretical values of −9.72 dB by no more than 0.03 dB. The maximum deviation of PSLR in range is less than 0.03 dB with respect to the theoretical value of −13.26 dB. This validates that the proposed frequency domain approach can accurately simulate the bistatic FMCW SAR signal.

Furthermore, the bistatic FMCW SAR raw signal simulation approach is validated by simulating the raw signal of an actual scene. In this experiment, we used the backscattering coefficients of a pulsed bistatic SAR image produced in [24]. This image was acquired by

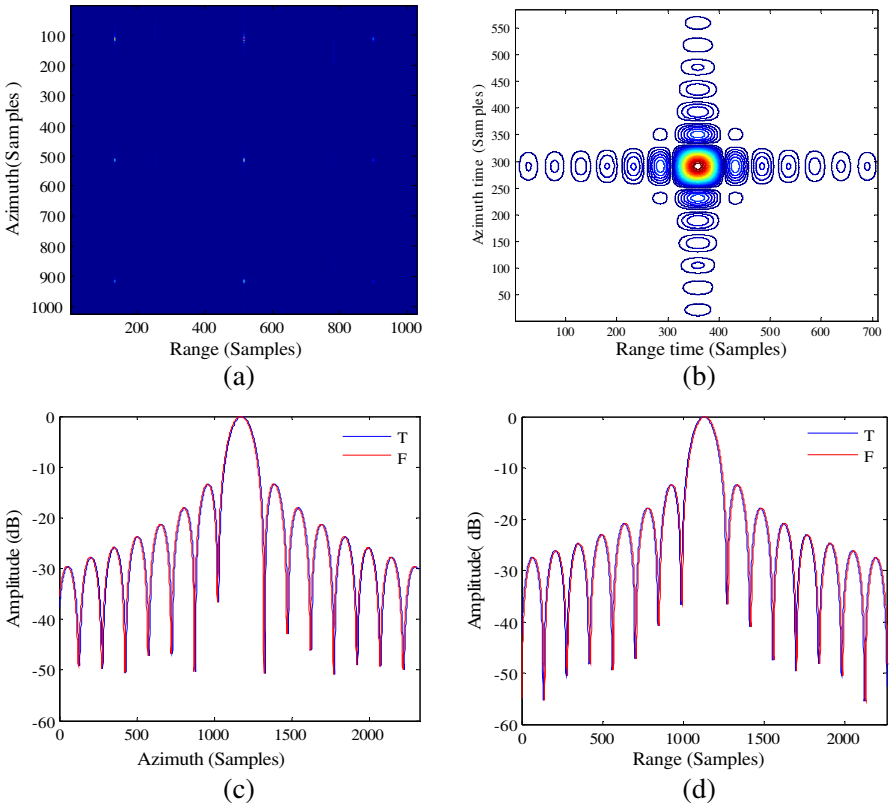

Figure 5. (a) The processing result of raw signal simulated by the proposed frequency domain approach. (b) Impulse response of PT9. (c)–(d) Comparison with the result of time domain method.

Table 2. Measurements of target PT9.

	Azimuth	Range
IRW	0.305 m	0.302 m
PSLR	−13.25 dB	−13.26 dB
ISLR	−9.73 dB	−9.72 dB

the spaceborne/airborne bistatic SAR experiments conducted in 2008 and 2009 by the Fraunhofer Institute for High Frequency Physics and Radar Techniques (FHR), employing the spaceborne radar system TerraSAR-X as the transmitter and the airborne radar system PAMIR as the separate receiver. The image we used covers an area at

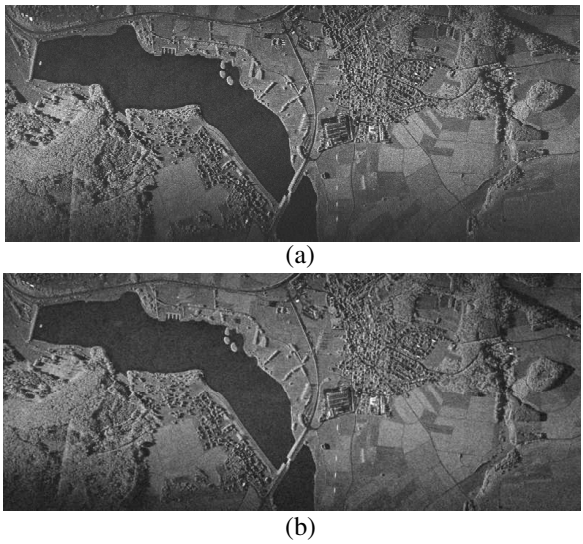

Figure 6. Image of an actual scene (Niederweidbach, Germany), obtained by (a) FHR's spaceborne/airborne bistatic SAR experiments; (b) by processing the simulated bistatic FMCW SAR raw signal via modified RDA. Near range is on the left.

Niederweidbach, Germany, which is shown in Fig. 6(a). The horizontal and vertical directions denote the range and the azimuth, respectively.

By locating the backscattering coefficients of the bistatic SAR image following the first step of the proposed approach, the desired reflectivity map is achieved. Based on the conceived reflectivity map, the raw signal of this area in bistatic FMCW SAR configuration is conceived following the simulation procedure as shown in Fig. 3. The simulation system parameters are listed in Table 1. Furthermore, the simulated raw signal is well-focused by the proposed RDA, the image is acquired as shown in Fig. 6(b). The processing result of the simulated raw signal is almost the same with the real physiognomy, without any geometrical deviation or spectrum aliasing, which proves the validation and accuracy of the simulated raw signal.

5. COMPUTATIONAL COMPLEXITY ANALYSES AND COMPARISON

To reveal the efficiency of the proposed frequency domain bistatic FMCW SAR scene simulator, the computational complexity of the proposed approach and traditional time domain simulation method

are calculated and compared.

In the case of time-domain bistatic FMCW SAR simulation, according to (6), the FMCW SAR raw signal is directly conceived by a twofold integral of reflectivity and impulse response functions, the number of floating point operations (FLOPs) of the time-domain simulation is

$$N_T = 5N_a^2 N_r^2 \tag{50}$$

In the case of the proposed frequency-domain bistatic FMCW SAR simulator, the bistatic FMCW SAR raw signal is conceived by carrying out CZT, interpolation and function multiplications, thus the number of FLOPs of the proposed approach is [36]

$$N_F = 10N_a N_r \log_2 N_a + 5N_a N_r \log_2 N_r + 24N_a N_r + 2N_a (N_r - 1) \tag{51}$$

By taking advantage of FFT operation, the proposed approach offers much lower computational complexity thus greatly reduces the calculation load. For further clarify and comparison, the FLOPs of the proposed approach and time-domain method are measured in giga-FLOPs (GFLOPs), respectively. The real FMCW SAR image in Section 5 is analyzed as an example. The image has 8192 pixels in the azimuth and 4096 pixels in the range. Thus we get,

$$\begin{cases} N_T = 5.63 \times 10^6 & \text{(GFLPOs)} \\ N_F = 7.25 & \text{(GFLPOs)} \end{cases} \tag{52}$$

Equation (52) demonstrates that the proposed approach provides great processing time reduction. This novel approach is proved to be precise and efficient, which renders bistatic FMCW SAR raw signal simulation of extended scenes feasible.

6. CONCLUSION

In this paper, an efficient bistatic FMCW SAR raw signal simulation approach for extended scene is proposed. It is the first time that a bistatic FMCW SAR simulator is conceived in the 2-D frequency domain. The approach is based on the CZT operation. By taking advantage of fast Fourier transform (FFT), the proposed raw signal simulation approach highly reduces the computational load with respect to a time domain approaches. The simulated bistatic FMCW SAR raw signal of a point targets and an actual scene (Niederweidbach, Germany) are used to valid the innovative algorithm, and achieved satisfying result. Numerical results demonstrate that the present approach can highly reduce the computational time significantly without accuracy loss while simulating extended scenes of bistatic FMCW SAR raw signal. The proposed raw signal simulator will really

help with the future development and application of bistatic FMCW SAR.

ACKNOWLEDGMENT

The work reported herein is jointly funded by the "hundred Talents Program" of the Chinese Academy of Sciences and General Program of the National Natural Science Foundation of China under grant of 61172122.

APPENDIX A.

This appendix is to calculate the phase error of the approximate formulation (31) in order to verify its accuracy.

Comparing (31) with the accurate spectrum formulation as shown in (21), the phase error of the approximate spectrum formulation is expressed as,

$$\begin{aligned}\Phi_{err}(f,f_\tau)=&\frac{2\pi(R_{0T}-R_{mR})}{c}\sqrt{(f_0+f)^2-\left(\frac{cf_{\tau T}}{v_T}\right)^2}\\&-\frac{2\pi\beta(R_{0R}-R_{mR})}{c}\left(D_Tf_0+\frac{1}{D_T}f\right)\\&+\frac{2\pi(R_{0R}-R_{mR})}{c}\left\{\sqrt{(f_0+f)^2-\left(\frac{cf_{\tau R}}{v_R}\right)^2}-D_Rf_0-\frac{1}{D_R}f\right\}\end{aligned}\quad\text{(A1)}$$

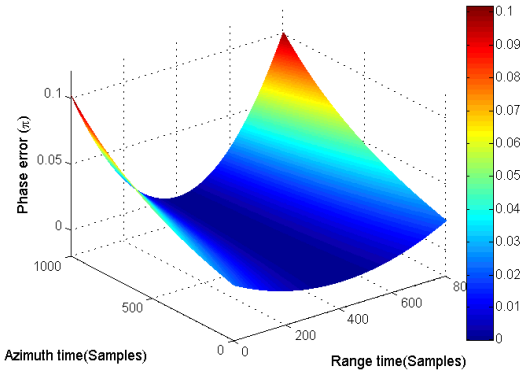

Figure A1. Maximal phase error of the reformulated spectrum model.

In the designed bistatic FMCW SAR configuration, as shown in Table 1, the maximal phase error is calculated and shown in Fig. A1. The phase error is much smaller than the acceptable level $\pi/4$, which proves that the approximate spectrum formulation is accurate enough in general bistatic FMCW SAR configuration.

REFERENCES

1. Meta, A., P. Hoogeboom, and L. P. Ligthart, "Signal processing for FMCW SAR," *IEEE Trans. Geosci. Remote Sens.*, Vol. 45, No. 11, Nov. 2007.
2. Lim, S. H., J. H. Han, S.-Y. Kim, and N.-H. Myung, "Azimuth beam pattern synthesis for airborne SAR system optimization," *Progress In Electromagnetics Research*, Vol. 106, 295–309, 2010.
3. Liu, Q., W. Hong, W. X. Tan, Y. Lin, Y. Wang, and Y. Wu, "An improved polar format algorithm with performance analysis for geosynchronous circular SAR 2D imaging," *Progress In Electromagnetics Research*, Vol. 119, 155–170, 2011.
4. Wei, X., P. Huang, and Y. K. Deng, "Multi-channel SPCMB-TOPS SAR for high-resolution wide-swath imaging," *Progress In Electromagnetics Research*, Vol. 116, 533–551, 2011.
5. Banasiak, R., R. Wajman, D. Sankowski, and M. Soleimani, "Three-dimensional nonlinear inversion of electrical capacitance tomography data using a complete sensor model," *Progress In Electromagnetics Research*, Vol. 100, 219–234, 2010.
6. Park, J.-I. and K.-T. Kim, "A comparative study on ISAR imaging algorithms for radar target identification," *Progress In Electromagnetics Research*, Vol. 108, 155–175, 2010.
7. Wei, S. J., X. L. Zhang, and J. Shi, "Linear array SAR imaging via compressed sensing," *Progress In Electromagnetics Research*, Vol. 117, 299–319, 2011.
8. Essen, H., H. H. Fuchs, and A. Pagels, "High resolution millimeterwave SAR for remote sensing of wave patterns," *Proc. GRASS*, 963–966, Barcelona, Spanish, Jun. 2007.
9. Edrich, M., "Design overview and flight test results of the miniaturized SAR sensor MISAR," *Proc. 1st EURAD*, 205–208, Amsterdam, The Netherlands, Oct. 2004.
10. Weib, M. and J. H. G. Ender, "A 3D imaging radar for small unmanned airplanes — ARTINO," *Proc. EURAD*, 209–212, Paris, France, Oct. 2005.

11. Ahmed, N., "Monostatic CW SAR concept for microsatellites," *EUSAR*, 1545–1554, Aachen, Germany, Jun. 2010.
12. Curlander, J. C. and R. N. Mcdonough, *Sythetic Aperture Radar: Systems and Signal Processing*, John Wiley & Sons, New York, 1991.
13. Krieger, G. and A. Moreira, "Spaceborne bi- and multistatic SAR: Potential and challenges," *IEE Proc. Radar Sonar Navig.*, Vol. 153, No. 3, 184–198, Jun. 2006.
14. Wu, J. J., J. Y. Yang, Y. L. Huang, Z. Liu, and H. G. Yang, "A new look at the point target reference spectrum for bistatic SAR," *Progress In Electromagnetics Research*, Vol. 119, 363–379, 2011.
15. Sun, J. P., S. Y. Mao, G. H. Wang, and W. Hong, "Extended exact transfer function algorithm for bistatic SAR of translational in variant case," *Progress In Electromagnetics Research*, Vol. 99, 89–108, 2009.
16. Sun, J., S. Mao, G. Wang, and W. Hong, "Polar format algorithm for spotlight bistatic SAR with arbitrary geometry configuration," *Progress In Electromagnetics Research*, Vol. 103, 323–338, 2010.
17. Ji, W. J. and C. M. Tong, "Bistatic scattering from two-dimensional dielectric ocean rough surface with a PEC object partially embedded by using the G-SMCG method," *Progress In Electromagnetics Research*, Vol. 105, 119–139, 2010.
18. Nies, H., O. Loffeld, and K. Natroshvili, "Analysis and focusing of bistatic airborne SAR data," *IEEE Trans. Geosci. Remote Sens.*, Vol. 45, No. 11, 3342–3349, Nov. 2007.
19. Crocco, L., F. Soldovieri, T. Millington, and N. J. Cass, "Bistatic tomographic GPR imaging for incipient pipeline leakage evaluation," *Progress In Electromagnetics Research*, Vol. 101, 307–321, 2010.
20. Qi, Y. L., W. X. Tan, Y. P. Wang, W. Hong, and Y. R. Wu, "3D bistatic OMEGA-K imaging algorithm for near range microwave imaging systems with bistatic planar scanning geometry," *Progress In Electromagnetics Research*, Vol. 121, 409–431, 2011.
21. Li, S., H. P. Xu, and L. Q. Zhang, "An advanced DSS-SAR InSAR terrain height estimation approach based on baseline decoupling," *Progress In Electromagnetics Research*, Vol. 119, 207–224, 2011.
22. Wang, R., O. Loffeld, Y. L. Neo, H. Nies, and Z. Dai, "Extending Loffeld's bistatic formula for the general bistatic SAR configuration," *IET Radar Sonar Navig.*, Vol. 4, 74–84, 2010.
23. Neo, Y. L., F. Wong, and I. G. Cumming, "A two-dimensional spectrum for bistatic SAR processing using series reversion,"

IEEE Geosci. Remote Sens. Lett., Vol. 4, No. 1, 93–96, Jan. 2007.

24. Wang, R., O. Loffeld, H. Nies, S. Knedlik, and J. H. G. Ender, "Chirp-scaling algorithm for bistatic SAR data in the constant-offset configuration," *IEEE Trans. Geosci. Remote Sens.*, Vol. 47, No. 3, 1296–1299, Mar. 2009.
25. Franceschetti, G., A. Iodice, S. Perna, and D. Riccio, "Efficient simulation of airborne SAR raw data of extended scenes," *IEEE Trans. Geosci. Remote Sens.*, Vol. 44, No. 10, 2851–2860, Oct. 2006.
26. Franceschetti, G., A. Iodice, S. Perna, and D. Riccio, "SAR sensor trajectory deviations: Fourier domain formulation and extended scene simulation of raw signal," *IEEE Trans. Geosci. Remote Sens.*, Vol. 44, No. 9, 2323–2334, Sep. 2006.
27. Jin, Y.-Q., "Polarimetric scattering modeling and information retrieval of SAR remote sensing — A review of FDU work," *Progress In Electromagnetics Research*, Vol. 104, 333–384, 2010.
28. Buddendick, H. and T. F. Eibert, "Bistatic image formation from shooting and bouncing rays simulated current distributions," *Progress In Electromagnetics Research*, Vol. 119, 1–18, 2011.
29. Franceschetti, G., R. Guida, A. Iodice, D. Riccio, G. Ruello, and U. Stilla, "Simulation tools for interpretation of high resolution SAR images of urban areas," *Proc. Urban Remote Sens. Joint Event*, 1–5, 2007.
30. Chang, Y. L., C. Y. Chiang, and K. S. Chen, "SAR image simulation with application to target recognition," *Progress In Electromagnetics Research*, Vol. 119, 35–57, 2011.
31. Zhang, M., Y. W. Zhao, H. Chen, and W. Q. Jiang, "SAR imaging simulation for composite model of ship on dynamic ocean scene," *Progress In Electromagnetics Research*, Vol. 113, 395–412, 2011.
32. Zhao, Y. W., M. Zhang, and H. Chen, "An efficient ocean SAR raw signal simulation by employing fast Fourier transform," *Journal of Electromagnetic Waves and Applications*, Vol. 24, No. 16, 2273–2284, 2010.
33. Wang, Y., Z. Zhang, and Y. Deng, "Squint spotlight SAR raw signal simulation in the frequency domain using optical principles," *IEEE Trans. Geosci. Remote Sens.*, Vol. 46, No. 8, 2208–2215, Aug. 2008.
34. Rabiner, L. R., R. W. Schafer, and C. M. Rader, "The chirp-Z transform and its applications," *IEEE Trans. Audio. Electro.*, Vol. 17, No. 2, 86–92, Jun. 1969.

35. Lanari, R., "A new method for the compensation of the SAR range cell migration based on the chirp Z-transform," *IEEE Trans. Geosci. Remote Sens.*, Vol. 33, No. 5, 1296–1299, Sep. 1995.
36. Cumming, I. G. and F. H. Wong, *Digital Processing of Synthetic Aperture Radar Data Algorithms and Implementation*, Artech House, Norwood, MA, 2005.